Carbon Dioxide Solubility in Phosphonium-based Deep Eutectic Solvents: an Experimental and Molecular Dynamics Study

Jingwen Wang,[a] Zhen Song,[b,c,*] Hongye Cheng,[a] Lifang Chen,[a] Liyuan Deng[d], Zhiwen Qi[a,*]

[a] *State Key Laboratory of Chemical Engineering, School of Chemical Engineering, East China University of Science and Technology, 130 Meilong Road, 200237, Shanghai, China*

[b] *Process Systems Engineering, Max Planck Institute for Dynamics of Complex Technical Systems, Sandtorstr. 1, D-39106 Magdeburg, Germany*

[c] *Process Systems Engineering, Otto-von-Guericke University Magdeburg, Universitätsplatz 2, D-39106 Magdeburg, Germany*

[d] *Department of Chemical Engineering, Norwegian University of Science and Technology, Sem Sælandsvei 4, 7491 Trondheim, Norway*

[*] *Corresponding authors: songz@mpi-magdeburg.mpg.de (Zhen Song), zwqi@ecust.edu.cn (Zhiwen Qi)*

ABSTRACT

Considering the great potential of deep eutectic solvent (DES) for CO_2 capture, this work studies the CO_2 solubility in DESs by combining experimental measurement and molecular dynamics (MD) simulation. First, four phosphonium-based DESs have been prepared in laboratory, involving two types of hydrogen bond acceptors (HBAs), namely tetrabutylphosphonium bromide (TBPB) and allyltriphenylphosphonium bromide (ATPPB), and two types of hydrogen bond donors (HBDs), namely phenol (PhOH) and diethylene glycol (DEG). The CO_2 solubility in the obtained DESs has been measured under 313.15 K – 333.15 K and pressure below 2000 kPa, and compared with that of previously reported DESs and ionic liquids. Second, MD simulations have been performed to study the microscopic behaviors of the involved DESs and mixtures. Through the analyses of radial distribution functions (RDFs), spatial distribution functions (SDFs) and intermolecular interaction energies, the eutectic formation and CO_2 absorption mechanisms, as well as the effect of HBA/HBD type and molar ratio are interpreted.

KEYWORDS: deep eutectic solvents, CO_2 solubility, molecular dynamics simulation

1. INTRODUCTION

Due to increasing concerns about the global warming issues, carbon dioxide (CO_2) capture and storage (CCS) has attracted significant attention in both the industry and academia.[1,2] At present, the most commonly used CO_2 capture technology in the industry is the chemical absorption by aqueous solutions of alkanolamines, such as monoethanolamine (MEA), diethanolamine (DEA), and methyldiethanolamine (MDEA).[3,4] However, such process suffers from three serious disadvantages: (1) large solvent loss; (2) high energy penalty for solvent regeneration; (3) severe corrosion of equipment.[5] Therefore, from the green chemistry and sustainability point of view, searching environmentally benign and functionally competitive alternatives for alkanolamines is highly desirable.

In the past few years, ionic liquids (ILs) have been extensively studied as alternative solvents for CO_2 absorption due to their unique physicochemical properties such as negligible vapor pressure, broad liquid range, and high chemical and thermal stability.[6-15] For example, Liu et al.[16] reported that the single-stage and multi-stage CO_2 absorption processes using [Bmim][Tf_2N] reduced the total energy consumption by 42.8% and 66.04%, respectively, comparing with that of the reference MDEA process. Similar results were also observed by Shiflett et al.[17,18] and Valencia-Marquez et al.,[19] demonstrating the energy- and cost-efficient merits of IL-based CO_2 capture processes. Nevertheless, the industrial application of ILs still faces the following challenges: (1) the synthesis and purification of ILs, especially functional ILs, is complex and expensive; (2) the health, safety, and environmental (HSE) influences of ILs are not yet fully revealed.[20-22]

To address the shortcomings of ILs, deep eutectic solvents (DESs) have been recently thrust into the limelight.[23-25] Bearing similar physicochemical properties as ILs, DESs are usually considered as “IL analogues”.[26] In addition, DESs can be prepared easily by mixing a hydrogen bond donor (HBD) with a hydrogen bond acceptor (HBA), without requiring any

complex synthesis and purification steps. More interestingly, a large number of cheap and renewable compounds can act as the HBD or HBA for forming DES, which makes this spectrum of solvent more affordable and sustainable than ILs.[27,28] Because of these attractive characteristics, DESs are widely expected as promising solvents for various chemical processes,[29-32] among which CO_2 absorption is of particular interest. Li et al.[33] firstly measured the CO_2 solubility in the eutectic mixtures of choline chloride (ChCl, act as HBA) and urea (act as HBD) with molar ratios of 1:1.5, 1:2 and 1:2.5, as a function of pressure up to 13000 kPa and temperature ranging from 313.15 K to 333.15 K. Afterwards, Leron and Li[34-36] reported the CO_2 solubility in DESs formed by mixing ChCl and HBDs of glycerol, urea, and ethylene glycol at the ratio of 1:2. The CO_2 solubility in other ChCl-based DESs with HBDs of dihydric alcohols (i.e., 1,4-butanediol, 2,3-butanediol, 1,2-propanediol), levulinic acid, and furfuryl alcohol was also investigated.[30,37]

Despite the progress made, the previous research has only covered a small number of DESs, mostly the ChCl-based ones. In this sense, there is a large room for extending the applicability of DES-based CO_2 capture process by testing different HBAs and HBDs. Moreover, except experimental measurement of the CO_2 absorption capacity and physicochemical properties of DESs, very little work has focused on the deep insight into the microscopic behaviors of DESs and {DES+CO_2} mixtures. Such insights, however, are of great significance for understanding the CO_2 absorption mechanisms of DESs and guiding the selection of DES components.[38-40]

Taking account of all the aforementioned aspects, this contribution presents an experimental and molecular dynamics (MD) study on the CO_2 solubility in DESs. As phosphonium-based DESs are suggested to have high CO_2 solubility capacities,[41-43] four phosphonium-based DESs have been covered in this work (see Section 3), which are for the

first time introduced for this application. The CO_2 solubility in these DESs has been measured experimentally and relevant thermodynamic properties have been correlated. MD simulations have then been carried out for the DESs and {DES + CO_2} systems, thereby providing insights into the CO_2 absorption behaviors from the microscopic level.

2. METHOD DESCRIPTION

2.1. Chemicals

CO_2 with a mole fraction of 0.99999 is supplied by Shanghai Wetry Standard Reference Gas Co., Ltd., China. For the preparation of DESs, two salt HBAs, tetrabutylphosphonium bromide (TBPB) and allyltriphenylphosphonium bromide (ATPPB), and two widely reported HBDs, namely phenol (PhOH) and diethylene glycol (DEG), were used. The information about the involved HBAs and HBDs is listed in Table 1. All chemicals are analytical grade reagents and used as received without further purification.

2.2. DES Preparation

The DESs studied in this work were simply prepared by mixing salts and HBDs at a certain ratio under atmospheric pressure and 313.15 K. After stirring for 3 h, the "mixture" was inspected visually to make sure that a homogenous DES was obtained. The concentration of water in each prepared DES was determined using Karl Fisher titration analysis (AQV-300, Hiranuma, Japan). The density of DESs was measured by a digital density meter (Anton Par, DMA-4500 M, Austria) with an accuracy of $\pm 5\times10^{-5}$ g·cm^{-3}.

2.3. CO_2 Solubility Measurement

The solubility of CO_2 in DESs was determined through the pressure drop method by using the apparatus illustrated in our previous work.[44,45] The apparatus mainly consists of a gas absorption vessel and a gas reservoir, whose volumes are 28 ± 1 mL (V_{AV}) and 150 ± 1 mL

(V_{GR}), respectively. After introducing a known mass of DES (ω, weighted on an electronic balance, Sartorius/Germany, ±0.0001 g) into the absorption vessel, the whole system was controlled at 313.15 K by a water bath (± 0.1 K) and then evacuated to an initial pressure of P_0 (P_0 < 5 kPa) with a vacuum pump. Keeping the valve between gas reservoir and CO_2 cylinder open, the gas reservoir was charged with CO_2 up to pressure P_1, and then this valve was closed. Afterwards, the valve between absorption vessel and gas reservoir was opened, and CO_2 entered into the absorption vessel to be absorbed into DES. To accelerate the absorption, a magnetic stirrer was turned on at 15 r·min^{-1}. The equilibrium is considered to be reached after the pressure of absorption vessel (P_2) keeps constant for longer than 1 h. Due to the negligible vapor pressure of DESs, the gas phase is considered to be pure CO_2.[46] Therefore, the partial pressure of CO_2 before absorption (P_b) and at equilibrium (P_e) can be calculated as:

$$\begin{aligned} P_b &= P_1 - P_0 \\ P_e &= P_2 - P_0 \end{aligned} \tag{1}$$

The absorbed amount of CO_2 in DES (n_{CO_2}) is derived as:

$$n_{CO_2} = \rho_g(P_b)V_{GR} - \rho_g(P_e)V_{GR} - \rho_g(P_e)(V_{AV} - \omega/\rho_{DES}) \tag{2}$$

where $\rho_g(P_i)$ denotes the density of CO_2 in mol·cm^{-3} under pressure P_i, obtained from NIST Standard Reference Data. ρ_{DES} is the density of DES at 313.15 K in g·cm^{-3}.

As the molar quantity of DES n_{DES} is already known from its mass weight and molecular weight, the molar solubility of CO_2 in DESs (x_{CO_2}) can be determined as:

$$x_{CO_2} = \frac{n_{CO_2}}{n_{CO_2} + n_{DES}} \tag{3}$$

In physical absorption cases, the measured CO_2 solubility in DESs can be used to derive the Henry's law constant based on mole fraction (H_x) as follows,

$$H_x(T,P) = \lim_{x_{CO_2}\to\infty} \frac{f^L_{CO_2}(T,P)}{x_{CO_2}}$$
$$= \lim_{x_{CO_2}\to\infty} \frac{P\phi_{CO_2}(T,P)}{x_{CO_2}} \quad (4)$$
$$= \frac{P_e}{x_{CO_2}}$$

where $f^L_{CO_2}$ is the fugacity of CO_2, ϕ_{CO_2} is the fugacity coefficient, and P_e is the pressure of the system at equilibrium. Under the moderate pressure range studied in this work, $f^L_{CO_2}$ is assumed to equal P_e. By correlating Henry's law constants, other important thermodynamic properties such as solution Gibb free energy ($\Delta_{sol}G$), solution enthalpy ($\Delta_{sol}H$), and solution entropy ($\Delta_{sol}S$) can be determined as:

$$\Delta_{sol}G = RT\ln(H(T,P))/p^0 \quad (5)$$

$$\Delta_{sol}H = R\left(\frac{\partial \ln(H(T,P)/p^0}{\partial(1/T)}\right)_p \quad (5)$$

$$\Delta_{sol}S = (\Delta_{sol}H - \Delta_{sol}G)/T \quad (6)$$

where p^0 refers to the standard pressure of 0.1 MPa.

2.4. MD Simulation

MD simulations were carried out for fresh DESs and {DESs + CO_2} systems (according to the experimentally measured CO_2 solubility). All the geometric optimizations of the salts, HBDs and CO_2 molecules were performed at the B3LYP/6-31++G** theoretical level using Gaussian 09 (version D.01), and then partial atomic charges were derived from the optimized geometry using the RESP method.[47] The structures and atom labels of the HBAs, HBDs, and CO_2 are presented in Figure S1 with the fitted partial atomic charges provided in Table S1 (Supporting Information). The force field parameters for involved molecules were all obtained from the amber force field. Temperature and pressure were scaled with V-rescale thermostat

and Parrinello-Rahman barostat, whose coupling time constant were 0.1 and 4.0 ps, respectively. The cutoff distance of the neighbor searching was set to be 1.5 nm, beyond which the long-range electrostatic interactions were computed using the particle mesh Ewald (PME) method with a grid spacing of 0.16 nm and fourth-order interpolation. Lorentz-Berthelot mixing rules are used for Lennard-Jones terms and a leap-frog algorithm with a time step of 1 fs is used to integrate the equations of motion. All the simulations were performed in an isothermal-isobaric ensemble (NPT) using the GROMACS code.[38] In the case of fresh DES, 300 HBA ion pairs plus a certain number of HBD molecules according to the stoichiometry are considered for simulations in the temperature range of 293.15 K to 333.15 K at 100 kPa. The {DESs + CO_2} system was prepared at 313.15 K under different absorption pressures, which contains the same number of HBA ion pairs and HBD molecules as that in the fresh DES simulation. These systems were performed starting from these initial boxes being equilibrated for 3 ns and the last 1 ns is used to collect data for radial distribution function (RDF) and spatial distribution function (SDF) analysis.

2.5. ^{13}CNMR Characterization

^{13}CNMR spectra of the two samples, fresh DES (ATPPB:PhOH (1:4)) before CO_2 absorption and {ATPPB:PhOH (1:4) + CO_2} system after CO_2 absorption, were recorded by a Bruker AV400 NMR spectrometer using $CDCl_3$ as a solvent and tetramethylsilane (TMS) as an internal standard.

3. RESULTS AND DISCUSSION

3.1 CO_2 solubility in DESs

Before performing CO_2 solubility experiments, the different combinations of HBAs and HBDs were tested to check the formation of DESs. An HBA to HBD ratio of 1:4 was selected

here for two reasons: (1) a small ratio of salt is favorable as it is the more expensive component of DES; (2) this mole ratio is quite common among ammonium and phosphonium salt based DESs reported previously.[42,48] It is found that the two HBDs, i.e., DEG and PhOH, can all form a homogeneous eutectic mixture with TBPB, whereas only PhOH is able to form DES with ATPPB. Additionally, for the combination of ATPPB and PhOH, a DES at the molar ratio of 1:6 was also prepared in order to investigate the effect of HBA to HBD ratio. The information of the prepared DESs is listed in Table 2 together with the measured properties.

The experimentally determined CO_2 solubility in the studied DESs at different temperatures is tabulated in Table 3. As exemplified in Figure 1, the CO_2 solubility in the DESs grows almost linearly with increasing pressure and the extrapolation line basically passes through the origin of the coordinate, indicating a physical absorption of gases in solvents.[35-37] Moreover, it can be found that both the type and the molar ratio of HBA and HBD have a notable effect on the CO_2 solubility under identical conditions. To be specific, (1) by mixing with the same ratio of PhOH (1:4), the ATPPB based DES has a higher CO_2 solubility than the TBPB based one; (2) with different HBDs, the CO_2 solubility in the TBPB based DESs follows the ranking as PhOH < DEG; (3) the CO_2 solubility in ATPPB:PhOH types of DESs decreases slightly as the HBA:HBD mole ratio changes from 1:4 to 1:6.

The thermodynamic properties correlated from the measured CO_2 solubility are listed in Table 4. For CO_2 dissolution in the studied DESs, the positive values of $\Delta_{sol}G$ show that the absorption of CO_2 into DESs is a non-spontaneous process.[46,48] The negative $\Delta_{sol}H$ shows that the dissolution of CO_2 in such DESs is an exothermic process; the relatively smaller absolute values compared with common organic solvents (e.g., -85 $kJ \cdot mol^{-1}$ for CO_2 in MDEA) mean the easier regeneration of DESs.[49] The large negative $\Delta_{sol}S$ indicates the higher ordering degree of the liquid phase from a molecular level after CO_2 absorption.

Figure 2 compares the CO_2 solubility in the studied DESs with previously reported DESs and ILs in literature.[22,34-36,46,48,50-55] As shown in Figure 2a, the studied phosphonium salt based DESs possess a much higher CO_2 solubility than the ChCl-based DESs under the specified conditions. For example, at 313.15 K and around 500 kPa, the CO_2 solubility in the studied DESs ranges from 0.0483 for DES2 to 0.0608 for DES3, which is 1.7 – 2.2 times higher than the best ChCl-based DESs (0.0281 for ChCl:levulinic acid of 1:5); in comparison to the two previously reported DESs based on phosphonium salt, the DESs studied here also have a notably higher CO_2 solubility. From Figure 2b, at 313.15 K and around 1500 kPa, the studied DESs exhibit higher CO_2 solubility (0.1950 – 0.2134) than [Emim][$EtSO_4$] (0.1000), [*N*-bpy][BF_4] (0.1440) and [Bmim][DCA] (0.1582) as well as comparable CO_2 solubility as that of imidazolium-based ILs paired with anions of $[BF_4]^-$, $[PF_6]^-$,$[NO_3]^-$ and $[TFO]^-$ (0.1960 – 0.2340). Although the ILs based on anions of $[Ac]^-$, $[Tf_2N]^-$, and $[FAP]^-$ have a much higher CO_2 solubility than the studied DESs (0.2687 – 0.4960), such ILs either suffer from high energy consumption for solvent regeneration (due to chemical absorption) or are very expensive (due to the highly fluorinated anions). These encouraging comparisons indicate that the DESs reported in this work are promising solvent for CO_2 physical absorption.

3.2 Insight into CO_2 absorption by DESs

In this section, MD simulations are carried out to study the microscopic behaviors of DESs and {DES + CO_2} mixtures, thereby exploring the eutectic formation and absorption mechanism of DES as well as the effect of HBA/HBD nature and ratio. To begin with, as the force field parameterization is the prerequisite for MD simulation, its reliability is evaluated by comparing the experimentally determined and MD computed densities of DESs in the range of 293.15 K – 333.15 K. As shown in Figure 3, for the four studied DESs, the average absolute deviations between the experimental and computed density in the whole temperature

range are only 0.0004 g/cm^3, 0.0039g/cm^3, 0.0042g/cm^3, and 0.0020 g/cm^3. Such an excellent agreement indicates the satisfactory performance of the employed parameterization for describing the macroscopic properties of the studied systems.[40,56]

3.2.1 DES formation mechanism

To understand the formation mechanism of the studied DESs, the main structural features of them at the molecular level are analyzed from the site-site radial distribution function (RDF) and spatial distribution function (SDF). Figure 4 illustrates such RDF and SDF analyses with ATPPB:PhOH (1:4) as an example.

As depicted in Figure 4a, the first two maximum peaks for the RDFs between cation ($ATPP^+$) and anion (Br^-) are located near 2.9565 Å for the C-H1···Br and C-H18···Br pair (H1, H18 corresponding to hydrogen atoms in the -C-C=C allyl group, detailed in Figure S1), which are slightly shorter than 3.0375 Å for the C-HB···Br pair (HB denotes H atoms in the benzene rings: H3 – H17, see Figure S1). This fact implies that the main cation – anion interactions in the HBA occur between Br^- and the hydrogen atoms in -C-C=C group in $ATPP^+$, which may be attributed to the strong steric hindrance of the benzene rings in $ATPP^+$ cation. This surmise can be supported by the SDF analysis in Figure 4d, wherein Br^- anions have larger density cap around the -C-C=C group of the cation. Figures 4b and 4c show the site-site RDFs between PhOH molecules with Br^- anions and $ATPP^+$ cations, respectively. As seen, the first maximum peak in the case of PhOH – Br appears around 2.1465 Å between the O1-H6···Br pair (atom labels of PhOH shown in Figure S1), which is much less than the sums of the van der Waals radius of H and Br atoms (3.15 Å) and thus indicates the formation of hydrogen bond. This interaction distance is notably shorter than that in the case of PhOH – ATPP, that is, 2.9565 Å – 3.0375 Å for C-H1···O1, C-H18···O1, and C-HB···O1, suggesting the stronger interactions of PhOH with Br^- anions in the mixtures of ATPPB:PhOH (1:4). The

preferential PhOH – Br^- interactions over those for PhOH – ATPP are also confirmed from the corresponding SDF analyses, where Br^- is much more densely distributed around PhOH in comparison to $ATPP^+$ (Figures 4e and 4f).

In the RDF analyses for TBPB:PhOH (1:4), TBPB:DEG (1:4), and ATPPB:PhOH (1:6), the HBD – Br^- interactions are also found to be much stronger than the HBD – cation ones (see Figure S2, Supporting Information), which agrees well with the results for ATPPB:PhOH (1:4). Therefore, it could be concluded that the formation of the studied phosphonium salt based DESs can be mainly ascribed to the strong hydrogen bonds between HBD and the anion of HBA (Br^-).

3.2.2 CO_2 absorption mechanism of DESs

In order to understand the CO_2 absorption mechanism of DESs, the microscopic behaviors of {DES + CO_2} systems are further investigated. The influence of absorbed CO_2 molecules on the studied DES systems is first explored by comparing the RDFs of cation – anion, cation – HBD, and anion – HBD before and after CO_2 absorption. As seen in Figure 5, for the four DES systems, the shape and location of the first maximum peaks of $g(r)_{cation\text{-}anion}$, $g(r)_{cation\text{-}HBD}$, and $g(r)_{anion\text{-}HBD}$ after CO_2 absorption remain nearly unchanged compared to those before absorption (that is fresh DES), which is in good accordance with the minor changes in the intermolecular interaction energies of cation – anion, anion – HBD, and cation – HBD before and after absorbing CO_2. As compared in Table S2 (Supporting Information), the interaction energies of the cation – anion, cation – HBD and anion – HBD only decline less than 2.0% for these studied DES systems. These facts imply that these DESs are able to accommodate CO_2 molecules without remarkable structure rearrangement. Such MD calculation results can be evidenced by the ^{13}C-NMR spectra of fresh and CO_2-loaded DESs. For example, the ^{13}C-NMR spectrum of CO_2-loaded ATPPB:PhOH (1:4) keeps the same as that of fresh DES, where no

new chemical shift is found (see Figure S3, Supporting Information). These above results confirm that CO_2 molecules are physically absorbed by the studied DESs. In the following, ATPPB:PhOH (1:4) is taken to amplify the CO_2 absorption mechanism for these studiedDESs.

Figures 6 and 7 illustrate the RDFs and SDFs analyses of the {ATPPB:PhOH (1:4) + CO_2} system, respectively. As shown in Figure 6a, the site-site RDFs between CO_2 (CD atom) and $ATPP^+$ have notable peaks for the pairs of CD···HB, CD···H1, CD···H18, and CD···H19 at about 3.7 Å. Nonetheless, the much higher intensity of the first maximum peak for the CD···HB pair suggests that the CO_2 molecules interact preferentially with hydrogen atoms in the benzene rings. Correspondingly, CO_2 molecules placed around the benzene rings have a much larger density than those around the -C-C=C group, as seen from the SDFs in Figure 7a. One can also note from Figure 7a that CO_2 molecules are distributed majorly in the Br^--free void around $ATPP^+$ and thus do not perturb the Br^- distribution appreciably. As for the CD···Br pair, the RDF has an intense peak at 3.5235 Å, accounting for the interactions between Br^- and the positively charged CD atom (Figure 6b). In the case of CD – PhOH pair, the first maximum peaks appear in the order as $g(r)_{C\text{-}O1}$ (3.3615 Å) < $g(r)_{C\text{-}HB}$ (3.6045 Å) < $g(r)_{C\text{-}H6}$ (3.7665 Å), showing that the main interactions take place between the CO_2 molecule and the oxygen atom in the hydroxyl group as well as hydrogen atoms in the benzene ring. Therefore, it can be found from Figure 7b that CO_2 molecules have a large density cap next to the oxygen atom and around the benzene ring, which are also in the Br^--free void around PhOH. Figures 7a and 7b again verify that the DES structure is not rearranged noticeably by the absorbed CO_2 molecules, which agree well with the RDF analyses of DESs before and after CO_2 absorption. For the other three {DES + CO_2} systems (see Figure S4 – S6, Supporting Information), very similar RDF and SDF results are also obtained, which manifest alike CO_2 absorption mechanisms of the studied DESs.

3.2.3 Effect of the type and molar ratio of HBA and HBD

Moving beyond the DES formation and CO_2 absorption mechanism, the effect of the type and molar ratio of HBA and HBD can also be interpreted from the MD simulation results.

For analyzing the effect of HBA type, the RDFs of {TBPB:PhOH(1:4) + CO_2} and {ATPPB:PhOH (1:4) + CO_2} systems are compared. In these two cases, the RDFs and RDFs of the PhOH – CO_2 and Br – CO_2 pairs almost follow the same pattern (see Figures 6, 7 and S4, Supporting Information), and thus only those of the TBP^+ – CO_2 and $ATPP^+$ – CO_2 are compared. As shown in Figure 8, a sharp and intense peak of CD···HB is observed for the $ATPP^+$ – CO_2 pair; whereas the RDFs for TBP^+ – CO_2 pair only present much broader and weaker peaks (CD···H3/H5/H7). Such RDFs differences clearly demonstrate stronger interactions between $ATPP^+$ and CO_2 than those between TBP^+ and CO_2. Therefore, the higher CO_2 solubility in the ATPPB based DES than that in the TBPB based one can be understood.

Following a similar manner, the RDFs of {TBPB:PhOH (1:4) + CO_2} and {TBPB:DEG (1:4) + CO_2} systems are compared to clarify the effect of HBD type (Figure S4 and S5, Supporting Information). Figure 9 illustrates the main RDF differences for these two systems, lying in the HBD – CO_2 pair. For the DEG – CO_2 pair, the intense peaks of CD···O1 and CD···O2/O3 occur at about 3.1995 Å (atoms is labeled in Figure S1), which are notably shorter than those for the PhOH – CO_2 pair (3.3615 Å for CD···O1 and 3.7665 Å for CD···HB). Such comparison indicates that DEG has stronger interactions with CO_2 than PhOH; thus, TBPB:DEG (1:4) possesses a higher CO_2 solubility than TBPB:PhOH (1:4).

As the DESs ATPPB:PhOH (1:4) and ATPPB:PhOH (1:6) have the same components, the effect of HBA and HBD molar ratio on CO_2 solubility is analyzed from their individual contribution to the DES – CO_2 interactions. To this end, the intermolecular interaction energies of CO_2 with $ATPP^+$, Br^- and PhOH are calculated by MD and exemplified with the

{ATPPB:PhOH (1:4) + CO_2} systems under different CO_2 pressures at 313.15 K. As seen in Figure 10, the interaction energy of these three pairs follow the ranking of $ATPP^+$ > PhOH > Br^-, where the differences become stronger as the pressure increases. Combining the contribution of $ATPP^+$ and Br^-, the HBA plays a dominant role in the DES – CO_2 interactions. Therefore, it can be inferred that decreasing the ratio of HBA in ATPPB:PhOH DESs will lead to a lower CO_2 solubility, as observed for ATPPB:PhOH (1:4) and ATPPB:PhOH (1:6).

4. CONCLUSION

In this work, four phosphonium-based DESs, namely TBPB:PhOH (1:4), TBPB:DEG (1:4), ATPPB:PhOH (1:4), and ATPPB:PhOH (1:6), were prepared and their CO_2 solubility under 313.15 K – 333.15 K and pressure below 2000 kPa were measured experimentally. Compared with the DESs and ILs previously reported in the literature, the DESs studied in this work are found to have competitive CO_2 solubility as physical absorbent. MD simulations were performed to study the microscopic behaviors of the DESs and {DES + CO_2} mixtures. The formation of the studied phosphonium-based DESs is found to be mainly attributed to the strong hydrogen bond interactions between HBD (PhOH or DEG) and Br^-. The physical absorption of CO_2 is evidenced from the RDFs and SDFs analyses of DESs and {DES + CO_2} systems, where it is observed that the accommodation of CO_2 does not lead to appreciable structure rearrangement of DES. Additionally, the effect of the type and molar ratio of HBA and HBD are well interpreted from the RDF and interaction energy point of view. The encouraging results in this work demonstrate that DESs are very promising absorbents for CO_2 capture; to finally realize the industrial application, the CO_2 absorption-desorption performances, as well as the absorption selectivity should be studied in future work.

ASSOCIATED CONTENT

Supporting Information

Supporting information associated with this article can be found in the online version at ****.

ACKNOWLEDGEMENT

The financial support from National Natural Science Foundation of China (21576081, 21776074 and 2181101120) is greatly acknowledged.

REFERENCES

(1) Rubin, E. S.; Chen, C.; Rao, A. B. Cost and performance of fossil fuel power plants with CO_2 capture and storage. *Energy Policy*. **2007,** *35*, 4444-4454.

(2) Bachu, S. CO_2 storage in geological media: Role, means, status and barriers to deployment. *Prog. Energy Combust. Sci.* **2008,** *34*, 254-273.

(3) Mukherjee, S.; Kumar, P.; Hosseini, A.; Yang, A. D.; Fennell, P. Comparative Assessment of Gasification Based Coal Power Plants with Various CO_2 Capture Technologies Producing Electricity and Hydrogen. *Energy & Fuels*. **2014,** *28*, 1028-1040.

(4) Ziobrowski, Z.; Krupiczka, R.; Rotkegel, A. Carbon dioxide absorption in a packed column using imidazolium based ionic liquids and MEA solution. *Int. J. Greenhouse Gas Control*. **2016,** *47*, 8-16.

(5) Taib, M. M.; Murugesan, T. Solubilities of CO_2 in aqueous solutions of ionic liquids (ILs) and monoethanolamine (MEA) at pressures from 100 to 1600 kPa. *Chem. Eng. J*. **2012,** *181*, 56-62.

(6) Moya, C.; Palomar, J.; Gonzalez-Miquel, M.; Bedia, J.; Rodriguez, F. Diffusion Coefficients of CO_2 in Ionic Liquids Estimated by Gravimetry. *Ind. Eng. Chem. Res.* **2014,** *53*, 13782-13789.

(7) Li, J.; Dai, Z.; Usman, M.; Qi, Z.; Deng, L. CO_2/H_2 separation by amino-acid ionic liquids with polyethylene glycol as co-solvent. *J. Greenhouse Gas Control*. **2016,** *45*, 207-215.

(8) Wang, J.; Song, Z.; Cheng, H.; Chen, L.; Deng, L.; Qi, Z. Computer-aided design of ionic liquids as absorbent for gas separation exemplified by CO_2 capture cases. *ACS*

Sustainable Chem. Eng. **2018,** *6*, 12025-12035.

(9) Zhang, J.; Qin, L.; Peng, D.; Zhou, T.; Cheng, H.; Chen, L.; Qi, Z. COSMO-descriptor based computer-aided ionic liquid design for separation processes: part II: task-specific design for extraction processes. *Chem. Eng. Sci*. **2017,** *162*, 364-374.

(10) Taheri, M.; Dai, C. N.; Lei, Z. G. CO_2 capture by methanol, ionic liquid, and their binary mixtures: Experiments, modeling, and process simulation. *AlChE J.* **2018,** *64*, 2168-2180.

(11) Song, Z.; Hu, X.; Zhou, Y.; Zhou, T.; Qi, Z.; Sundmacher, K. Rational design of double salt ionic liquids as extraction solvents: Separation of thiophene/n-octane as example. *AlChE J.* **2019,** *65*, e16625.

(12) Song, Z.; Zhang, C.; Qi, Z.; Zhou, T.; Sundmacher, K. Computer-aided design of ionic liquids as solvents for extractive desulfurization. *AlChE J.* **2018,** *64*, 1013-1025.

(13) de Riva, J.; Ferro, V.; Moya, C.; Stadtherr, M. A.; Brennecke, J. F.; Palomar, J. Aspen Plus supported analysis of the post-combustion CO_2 capture by chemical absorption using the $[P_{2228}]$ [CNPyr] and $[P_{66614}]$ [CNPyr] AHA Ionic Liquids. *Int. J. Greenhouse Gas Control.* **2018,** *78*, 94-102.

(14) Zhao, Y.; Gani, R.; Afzal, R. M.; Zhang, X.; Zhang, S. Ionic liquids for absorption and separation of gases: An extensive database and a systematic screening method. *AlChE J.* **2017,** *63*, 1353-1367.

(15) Lei, Z. G.; Dai, C. N.; Song, W. J. Adsorptive absorption: A preliminary experimental and modeling study on CO_2 solubility. *Chem. Eng. Sci.* **2015,** *127*, 260-268.

(16) Liu, X. Y.; Huang, Y.; Zhao, Y. S.; Gani, R.; Zhang, X. P.; Zhang, S. J. Ionic Liquid Design and Process Simulation for Decarbonization of Shale Gas. *Ind. Eng. Chem. Res.* **2016,** *55*, 5931-5944.

(17) Shiflett, M. B.; Drew, D. W.; Cantini, R. A.; Yokozeki, A. Carbon Dioxide Capture Using Ionic Liquid 1-Butyl-3-methylimidazolium Acetate. *Energy & Fuels*. **2010,** *24*, 5781-5789.

(18) Shiflett, M. B.; Shiflett, A. D.; Yokozeki, A. Separation of tetrafluoroethylene and carbon dioxide using ionic liquids. *Sep. Purif. Technol*. **2011,** *79*, 357-364.

(19) Valencia-Marquez, D.; Flores-Tlacuahuac, A.; Ricardez-Sandoval, L. Technoeconomic and Dynamical Analysis of a CO_2 Capture Pilot-Scale Plant Using Ionic Liquids. *Ind. Eng. Chem. Res*. **2015,** *54*, 11360-11370.

(20) Smiglak, M.; Reichert, W. M.; Holbrey, J. D.; Wilkes, J. S.; Sun, L. Y.; Thrasher, J. S.; Kirichenko, K.; Singh, S.; Katritzky, A. R.; Rogers, R. D. Combustible ionic liquids by design: is laboratory safety another ionic liquid myth? *Chem. Commun.* **2006,** 24, 2554-2556.

(21) Chen, L.; Sharifzadeh, M.; Mac Dowell, N.; Welton, T.; Shah, N.; Hallett, J. P. Inexpensive ionic liquids: $[HSO4]^-$-based solvent production at bulk scale. *Green Chem*. **2014,** *16*, 3098-3106.

(22) Sarmad, S.; Xie, Y. J.; Mikkola, J. P.; Ji, X. Y. Screening of deep eutectic solvents (DESs) as green CO_2 sorbents: from solubility to viscosity. *New J. Chem.* **2017,** *41*, 290-301.

(23) Ali, E.; Hadj-Kali, M. K.; Mulyono, S.; Alnashef, I. Analysis of operating conditions for CO_2 capturing process using deep eutectic solvents. *Int. J. Greenhouse Gas Control*. **2016,** *47*,

342-350.

(24) Hadj-Kali, M. K.; Mulyono, S.; Hizaddin, H. F.; Wazeer, I.; El-Blidi, L.; Ali, E.; Hashim, M. A.; AlItashef, I. M. Removal of Thiophene from Mixtures with n-Heptane by Selective Extraction Using Deep Eutectic Solvents. *Ind. Eng. Chem. Res*. **2016,** *55*, 8415-8423.

(25) Abbott, A. P.; Frisch, G.; Hartley, J.; Ryder, K. S. Processing of metals and metal oxides using ionic liquids. *Green Chem*. **2011,** *13*, 471-481.

(26) Smith, E. L.; Abbott, A. P.; Ryder, K. S. Deep Eutectic Solvents (DESs) and Their Applications. *Chem. Rev.* **2014,** *114*, 11060-11082.

(27) Abbott, A. P.; Boothby, D.; Capper, G.; Davies, D. L.; Rasheed, R. K. Deep eutectic solvents formed between choline chloride and carboxylic acids: Versatile alternatives to ionic liquids. *J Am Chem Soc*. **2004,** *126*, 9142-9147.

(28) Carriazo, D.; Serrano, M. C.; Gutierrez, M. C.; Ferrer, M. L.; del Monte, F. Deep-eutectic solvents playing multiple roles in the synthesis of polymers and related materials. *Chem. Soc. Rev.* **2012,** *41*, 4996-5014.

(29) Guo, W. J.; Hou, Y. C.; Wu, W. Z.; Ren, S. H.; Tian, S. D.; Marsh, K. N. Separation of phenol from model oils with quaternary ammonium salts via forming deep eutectic solvents. *Green Chem*. **2013,** *15*, 226-229.

(30) Oliveira, F. S.; Pereiro, A. B.; Rebelo, L. P. N.; Marrucho, I. M. Deep eutectic solvents as extraction media for azeotropic mixtures. *Green Chem*. **2013,** *15*, 1326-1330.

(31) Tang, X. D.; Zhang, Y. F.; Li, J. J. Alkylation of thiophenic compounds catalyzed by deep eutectic solvents. *Catal. Commun.* **2015,** *70*, 40-43.

(32) Qin, L.; Li, J. S.; Cheng, H. Y.; Chen, L. F.; Qi, Z. W.; Yuan, W. K. Association extraction for vitamin E recovery from deodorizer distillate by in situ formation of deep eutectic solvent. *AlChE J.* **2017,** *63*, 2212-2220.

(33) Li, X. Y.; Hou, M. Q.; Han, B. X.; Wang, X. L.; Zou, L. Z. Solubility of CO_2 in a choline chloride plus urea eutectic mixture. *J Chem Eng Data*. **2008,** *53*, 548-550.

(34) Leron, R. B.; Caparanga, A.; Li, M. H. Carbon dioxide solubility in a deep eutectic solvent based on choline chloride and urea at T=303.15 – 343.15 K and moderate pressures. *Journal of the Taiwan Institute of Chemical Engineers*. **2013,** *44*, 879-885.

(35) Leron, R. B.; Li, M. H. Solubility of carbon dioxide in a choline chloride-ethylene glycol based deep eutectic solvent. *Thermochim. Acta*. **2013,** *551*, 14-19.

(36) Leron, R. B.; Li, M. H. Solubility of carbon dioxide in a eutectic mixture of choline chloride and glycerol at moderate pressures. *J. Chem. Thermodyn.* **2013,** *57*, 131-136.

(37) Chen, Y. F.; Ai, N.; Li, G. H.; Shan, H. F.; Cui, Y. H; Deng, D. S. Solubilities of Carbon Dioxide in Eutectic Mixtures of Choline Chloride and Dihydric Alcohols. *J Chem Eng Data*. **2014,** *59*, 1247-1253.

(38) Sun, H.; Li, Y.; Wu, X.; Li, G. H. Theoretical study on the structures and properties of mixtures of urea and choline chloride. *J. Mol. Model.* **2013,** *19*, 2433-2441.

(39) Ullah, R.; Atilhan, M.; Anaya, B.; Khraisheh, M.; Garcia, G.; ElKhattat, A.; Tariq, M.; Aparicio, S. A detailed study of cholinium chloride and levulinic acid deep eutectic solvent system for CO_2 capture via experimental and molecular simulation approaches. *PCCP*. **2015,** *17*, 20941-20960.

(40) Altamash, T.; Atilhan, M.; Aliyan, A.; Ullah, R.; Garcia, G.; Aparicio, S. Insights into choline chloride-phenylacetic acid deep eutectic solvent for CO_2 absorption. *RSC Adv.* **2016,** *6*, 109201-109210.

(41) Ghaedi, H.; Ayoub, M.; Sufian, S.; Lal, B.; Shariff, A. M. Measurement and correlation of physicochemical properties of phosphonium-based deep eutectic solvents at several temperatures (293.15 K – 343.15 K) for CO_2 capture. *J. Chem. Thermodyn*. **2017,** *113*, 41-51.

(42) Ghaedi, H.; Ayoub, M.; Sufian, S.; Shariff, A. M.; Hailegiorgis, S. M. and Khan, S. N. CO_2 capture with the help of Phosphonium-based deep eutectic solvents. *J. Mol. Liq.* **2017,** *243*, 564-571.

(43) Ghaedi, H.; Ayoub, M.; Sufian, S.; Murshid, G.; Farrukh, S.; Shariff, A. M. Investigation of various process parameters on the solubility of carbon dioxide in phosphonium-based deep eutectic solvents and their aqueous mixtures: Experimental and modeling. *Int. J. Greenhouse Gas Control*. **2017,** *66*, 147-158.

(44) Li, J.; Ye, Y. M.; Chen, L. F.; Qi, Z. W. Solubilities of CO_2 in Poly(ethylene glycols) from (303.15 to 333.15) K. *J Chem Eng Data*. **2012,** *57*, 610-616.

(45) Li, J.; Chen, L.; Ye, Y.; Qi, Z. Solubility of CO2 in the mixed solvent system of alkanolamines and poly(ethylene glycol) 200. J Chem Eng Data. **2014**, *59*, 1781-1787.

(46) Lu, M. Z.; Han, G. Q.; Jiang, Y. T.; Zhang, X. D.; Deng, D. S.; Ai, N. Solubilities of carbon dioxide in the eutectic mixture of levulinic acid (or furfuryl alcohol) and choline chloride. *J. Chem. Thermodyn.* **2015,** *88*, 72-77.

(47) Xing, H.; Zhao, X.; Yang, Q.; Su, B.; Bao, Z.; Yang, Y.; Ren, Q. Molecular Dynamics

Simulation Study on the Absorption of Ethylene and Acetylene in Ionic Liquids. *Ind. Eng. Chem. Res*. **2013,** *52*, 9308-9316.

(48) Liu, X. B.; Gao, B.; Jiang, Y. T.; Ai, N.; Deng, D. S. Solubilities and Thermodynamic Properties of Carbon Dioxide in Guaiacol-Based Deep Eutectic Solvents. *J Chem. Eng. Data*. **2017,** *62*, 1448-1455.

(49) Peng, D. L.; Zhang, J. A.; Cheng, H. Y.; Chen, L. F.; Qi, Z. W. Computer-aided ionic liquid design for separation processes based on group contribution method and COSMO-SAC model. *Chem. Eng. Sci.* **2017,** *159*, 58-68.

(50) Li, G. H.; Deng, D. S.; Chen, Y. F.; Shan, H. F.; Ai, N. Solubilities and thermodynamic properties of CO_2 in choline-chloride based deep eutectic solvents. *J. Chem. Thermodyn.* **2014,** *75*, 58-62.

(51) Aki, S. N. V. K.; Mellein, B. R.; Saurer, E. M.; Brennecke, J. F. High-pressure phase behavior of carbon dioxide with imidazolium-based ionic liquids. *J. Phys. Chem. B*. **2004,** *108*, 20355-20365.

(52) Blanchard, L. A.; Gu, Z. Y.; Brennecke, J. F. High-pressure phase behavior of ionic liquid/CO_2 systems. *J. Phys. Chem. B*. **2001,** *105*, 2437-2444.

(53) Muldoon, M. J.; Aki, S. N. V. K.; Anderson, J. L.; Dixon, J. K.; Brennecke, J. F. Improving carbon dioxide solubility in ionic liquids. *J. Phys. Chem. B*. **2007,** *111*, 9001-9009.

(54) Shiflett, M. B.; Niehaus, A. M. S.; Elliott, B. A.; Yokozeki, A. Phase Behavior of N_2O and CO_2 in Room-Temperature Ionic Liquids [bmim][Tf_2N], [bmim][BF_4], [bmim][$N(CN)_2$], [bmim][Ac], [eam][NO_3], and [bmim][SCN]. *Int. J. Thermophys.* **2012,** *33*, 412-436.

(55) Yokozeki, A.; Shiflett, M. B.; Junk, C. P.; Grieco, L. M.; Foo, T. Physical and Chemical Absorptions of Carbon Dioxide in Room-Temperature Ionic Liquids. *J. Phys. Chem. B*. **2008,** *112*, 16654-16663.

(56) Koddermann, T.; Paschek, D.; Ludwig, R. Molecular dynamic simulations of ionic liquids: A reliable description of structure, thermodynamics and dynamics. *Chemphyschem*. **2007,** *8*, 2464-2470.

Table Captions

Table 1. Information of chemicals used in this work.

Table 2. Information of the prepared DESs in this work.

Table 3. Solubility of CO_2 in the studied DESs at 313.15 – 333.15 K.

Table 4. Henry's law constants (H_x) and correlated thermodynamic properties of CO_2 in the studied DESs.

Table 1

Chemicals	Suppliers	Mass fraction purity
TBPB	Lanzhou Institute of Chemical Physics	≥ 99.0%
ATPPB	Shanghai Aladdin Chemical Reagent	≥ 99.0%
PhOH	Shanghai Titan Scientific	≥ 99.0%
DEG	Shanghai Aladdin Chemical Reagent	≥ 99.0%

Table 2

Solutions	HBA	HBD	Molar ratio	Water content (wt%)	T (K)	ρ (g·cm^{-3})
DES1	TBPB	PhOH	1:4	0.5891	293.15	1.0734
					303.15	1.0662
					313.15	1.0592
					323.15	1.0522
					333.15	1.0457
DES2	TBPB	DEG	1:4	1.2730	293.15	1.0891
					303.15	1.0825
					313.15	1.0758
					323.15	1.0691
					333.15	1.0625
DES3	ATPPB	PhOH	1:4	0.3490	293.15	1.1730
					303.15	1.1657
					313.15	1.1585
					323.15	1.1514
					333.15	1.1443
DES4	ATPPB	PhOH	1:6	0.2544	293.15	1.1582
					303.15	1.1571
					313.15	1.1434
					323.15	1.1362
					333.15	1.1291

Table 3

T=313.15K		323.15K		333.15K	
		DES1			
x_{CO2}	P/kPa	x_{CO2}	P/kPa	x_{CO2}	P/kPa
0.0291	234.5	0.0188	163.8	0.0184	203.4
0.0529	463.6	0.0400	399.0	0.0413	481.2
0.0953	737.0	0.0679	608.4	0.0585	601.7
0.1232	932.0	0.0916	786.9	0.0886	856.0
0.1573	1188.8	0.1237	1018.7	0.1157	1024.7
0.2048	1578.5	0.1503	1241.2	0.1430	1272.9
		DES2			
0.0236	183.5	0.0130	94.4	0.0169	164.8
0.0483	379.8	0.0283	270.7	0.0413	397.4
0.0887	621.6	0.0638	464.2	0.0773	642.3
0.1325	892.3	0.0974	700.8	0.1187	903.8
0.1567	1024.5	0.1296	895.4	0.1514	1103.6
0.2123	1398.1	0.1677	1148.0	0.1954	1396.5
		DES3			
0.0300	218.2	0.0341	231.4	0.0203	182.7
0.0608	397.4	0.0485	415.3	0.0530	472.8
0.0995	631.6	0.0875	683.8	0.0777	664.5
0.1426	886.6	0.1248	904.6	0.1034	821.3
0.1781	1093.3	0.1649	1125.7	0.1414	1066.4
0.2134	1333.2	0.1974	1325.9	0.1795	1345.1
		DES4			
0.0245	183.3	0.0217	159.9	0.0212	191.2
0.0590	409.8	0.0459	327.3	0.0520	457.2
0.0910	669.0	0.0781	567.9	0.0781	700.8
0.1286	871.7	0.0940	818.9	0.0985	978.4
0.1656	1098.5	0.1282	1088.3	0.1167	1123.6
0.1950	1320.3	0.1630	1328.9	0.1475	1387.3

Table 4

	H_x (MPa)			Δsol G (kJ·mol^{-1})	Δsol H (kJ·mol^{-1})	Δsol S (J·mol^{-1}·K^{-1})
	313.15 K	323.15 K	333.15 K	313.15 K	-	313.15 K
DES1	7.90	8.75	9.43	12.86	-15.88	-91.78
DES2	6.72	7.51	8.29	11.85	-16.27	-89.80
DES3	6.46	7.33	8.24	11.61	-18.44	-95.96
DES4	6.99	7.85	8.65	12.10	-17.21	-93.60

Figure Captions

Figure 1 Solubility of CO_2 in DESs at 313.15 K as a function of pressure (symbols, experimental; lines, linear fit).

Figure 2 Comparison of CO_2 solubility in the DESs studied in this work with previously reported (a) DESs under around 500 kPa and (b) ILs under around 1500 kPa at 313.15 K.

Figure 3 Comparison of experimentally measured (symbols) and the MD calculated (lines) density of the studied DESs.

Figure 4 RDFs of (a) $ATPP^+$ – Br^-, (b) Br^- – PhOH, and (c) $ATPP^+$ – PhOH, and SDFs of (d) Br^- around $ATPP^+$ (3-times bulk density), (e) Br^- around PhOH (3-times bulk density), and (f) $ATPP^+$ around PhOH (0.3-times bulk density) for ATPPB:PhOH (1:4).

Figure 5 RDFs for cation – anion, anion – HBD, and cation – HBD of the four studied DESs before and after absorption of CO_2.

Figure 6 RDFs of (a) CO_2 – $ATPP^+$ (b) CO_2 – $ATPP^+$ and CO_2 – PhOH in the {ATPPB:PhOH (1:4) + CO_2} system.

Figure 7 SDFs of CO_2 (ice blue) and Br^- anions (green) around (a) $ATPP^+$ and (b) PhOH in the {ATPPB:PhOH (1:4) + CO_2} system (3-times bulk density).

Figure 8 RDFs of CO_2 – cation in the {ATPPB:PhOH (1:4) + CO_2} and {TBPB:PhOH (1:4) + CO_2} systems.

Figure 9 RDFs of CO_2 – HBD in the {TBPB:PhOH (1:4) + CO_2} and {TBPB:DEG (1:4) + CO_2} systems.

Figure 10 Intermolecular interaction energy between CO_2 and $ATPP^+$/Br^-/PhOH in the {ATPPB:PhOH (1:4) + CO_2} system.

Figure 1

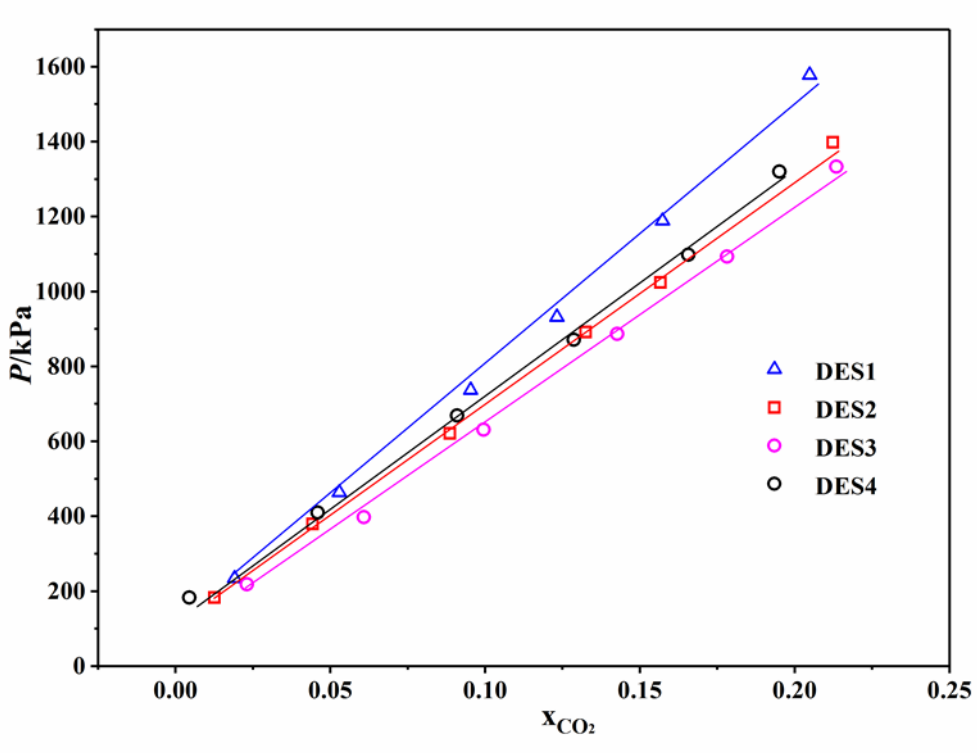
1600
1400
1200
1000
800
600
400
200
0
P/kPa
0.00
0.05
0.10
0.15
0.20
0.25
x_{CO_2}
DES1
DES2
DES3
DES4

Figure 2

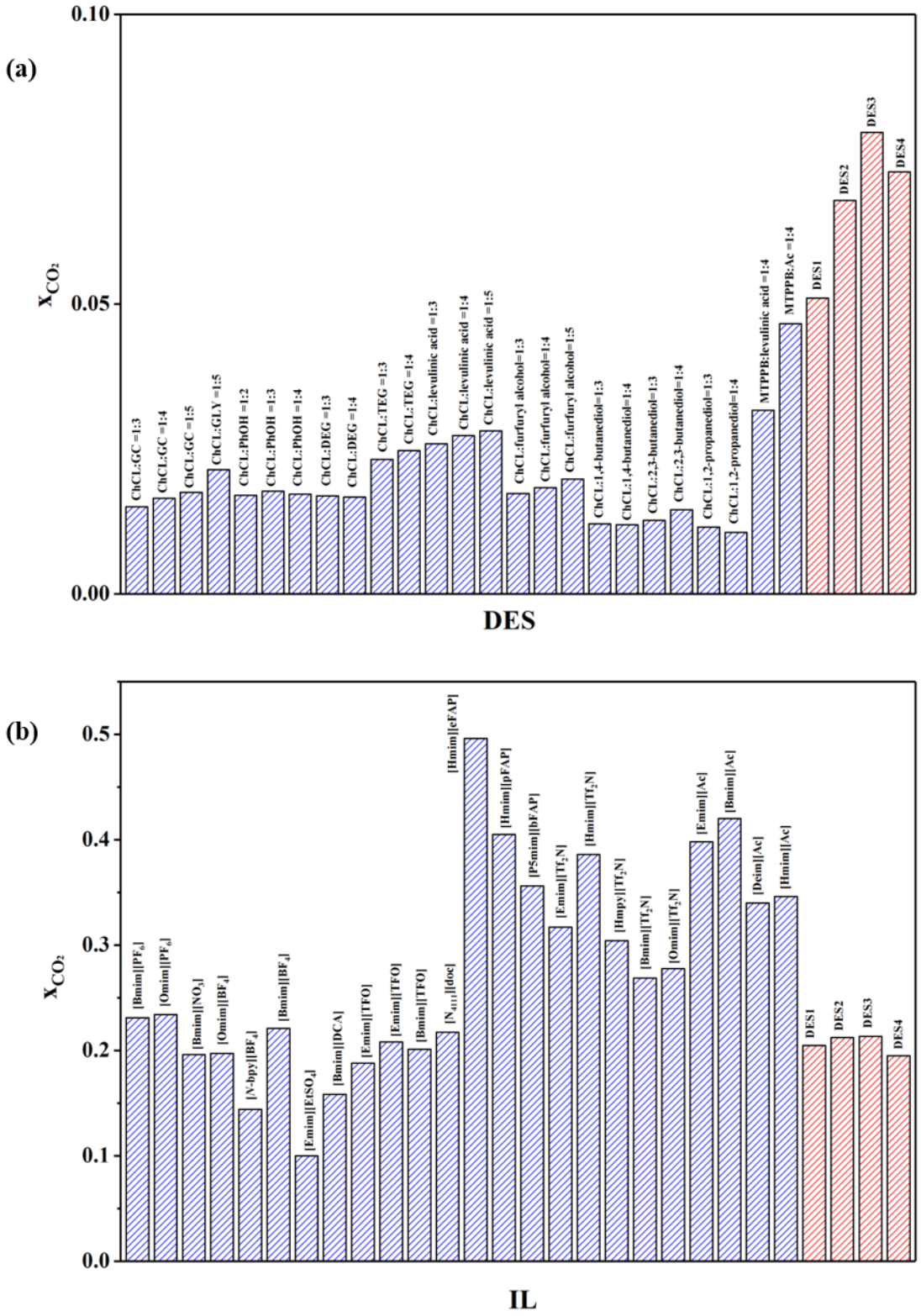
(a)
0.10
0.05
0.00
X_{CO_2}
ChCL:GC =1:3
ChCL:GC =1:4
ChCL:GC =1:5
ChCL:GLY =1:5
ChCL:PhOH =1:2
ChCL:PhOH =1:3
ChCL:PhOH =1:4
ChCL:DEG =1:3
ChCL:DEG =1:4
ChCL:TEG =1:3
ChCL:TEG =1:4
ChCL:levulinic acid =1:3
ChCL:levulinic acid =1:4
ChCL:levulinic acid =1:5
ChCL:furfuryl alcohol=1:3
ChCL:furfuryl alcohol=1:4
ChCL:furfuryl alcohol=1:5
ChCL:1,4-butanediol=1:3
ChCL:1,4-butanediol=1:4
ChCL:2,3-butanediol=1:3
ChCL:2,3-butanediol=1:4
ChCL:1,2-propanediol=1:3
ChCL:1,2-propanediol=1:4
MTPPB:levulinic acid =1:4
MTPPB:Ac =1:4
DES1
DES2
DES3
DES4
DES
(b)
0.5
0.4
0.3
0.2
0.1
0.0
X_{CO_2}
[Bmim][PF_6]
[Omim][PF_6]
[Bmim][NO_3]
[Omim][BF_4]
[N-bpy][BF_4]
[Bmim][BF_4]
[Emim][$EtSO_4$]
[Bmim][DCA]
[Emim][TFO]
[Emim][TFO]
[Bmim][TFO]
[N_{111}][doc]
[Hmim][eFAP]
[Hmim][pFAP]
[P5mim][bFAP]
[Emim][Tf_2N]
[Hmim][Tf_2N]
[Hmpy][Tf_2N]
[Bmim][Tf_2N]
[Omim][Tf_2N]
[Emim][Ac]
[Bmim][Ac]
[Deim][Ac]
[Hmim][Ac]
DES1
DES2
DES3
DES4
IL

Figure 3

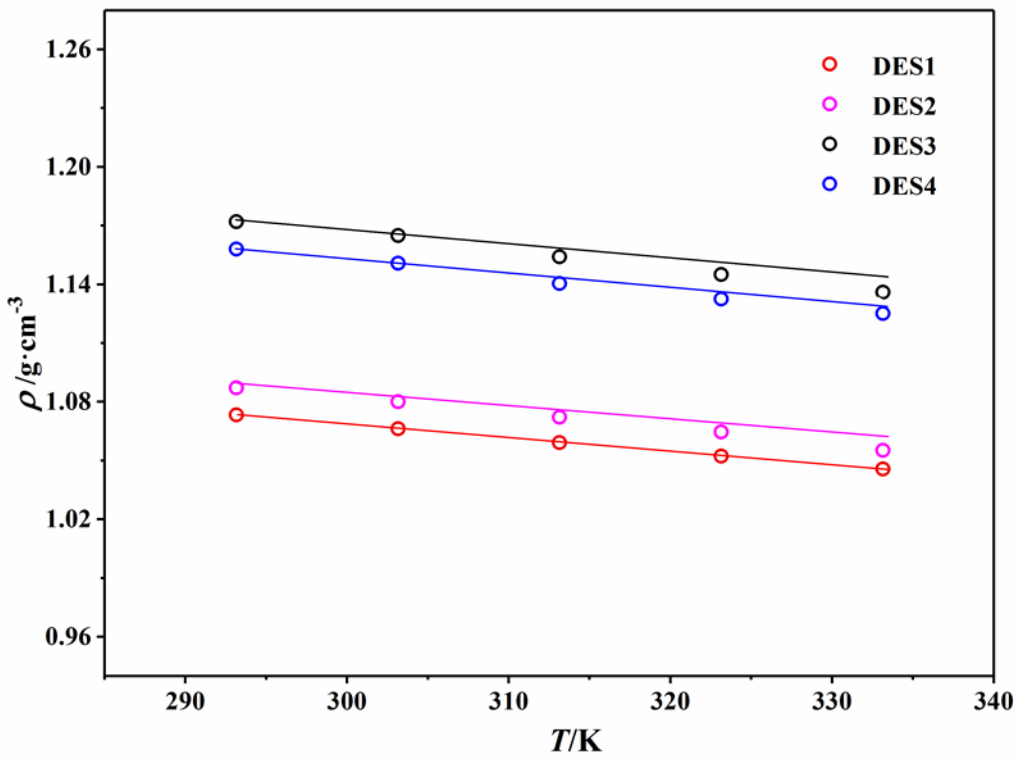
DES1
DES2
DES3
DES4
1.26
1.20
1.14
1.08
1.02
0.96
ρ /g·cm-3
290
300
310
320
330
340
T/K

Figure 4

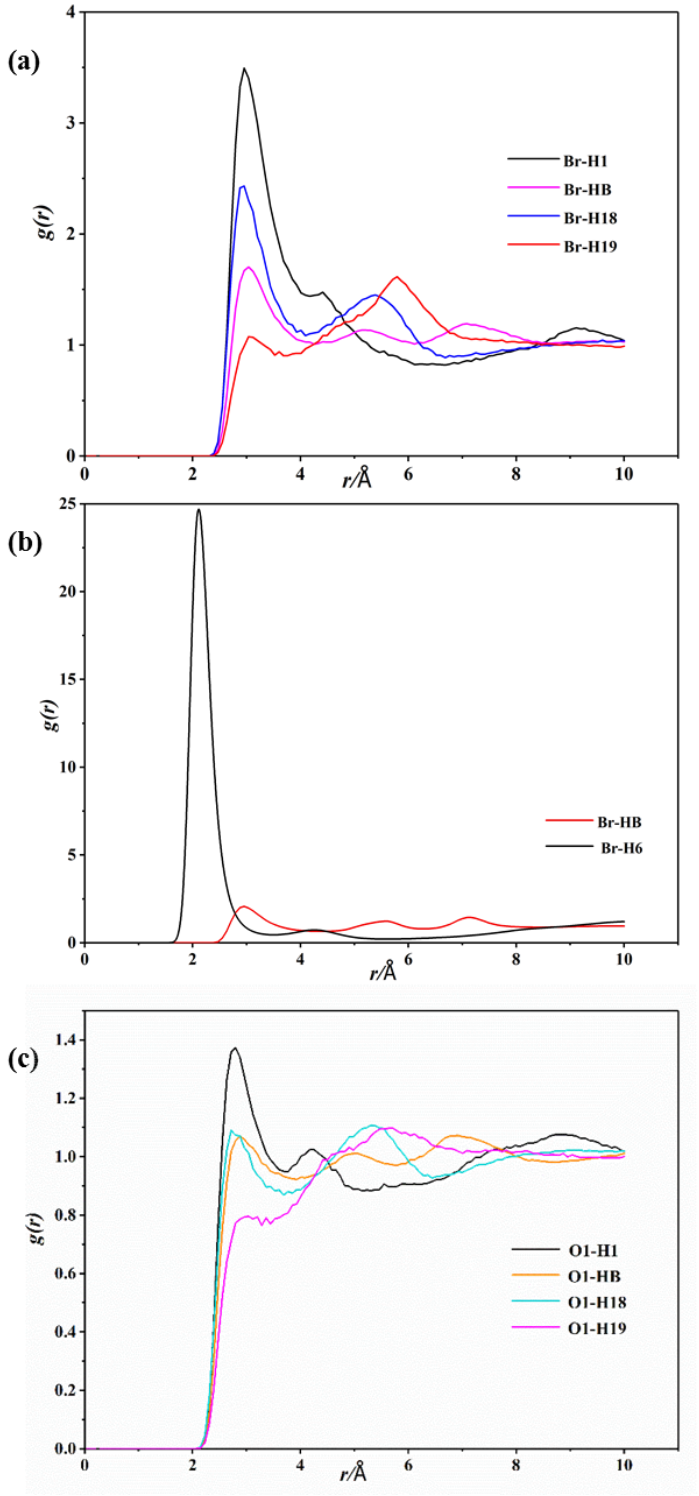
(a)
g(r)
r/Å
Br-H1
Br-HB
Br-H18
Br-H19
(b)
g(r)
r/Å
Br-HB
Br-H6
(c)
g(r)
r/Å
O1-H1
O1-HB
O1-H18
O1-H19

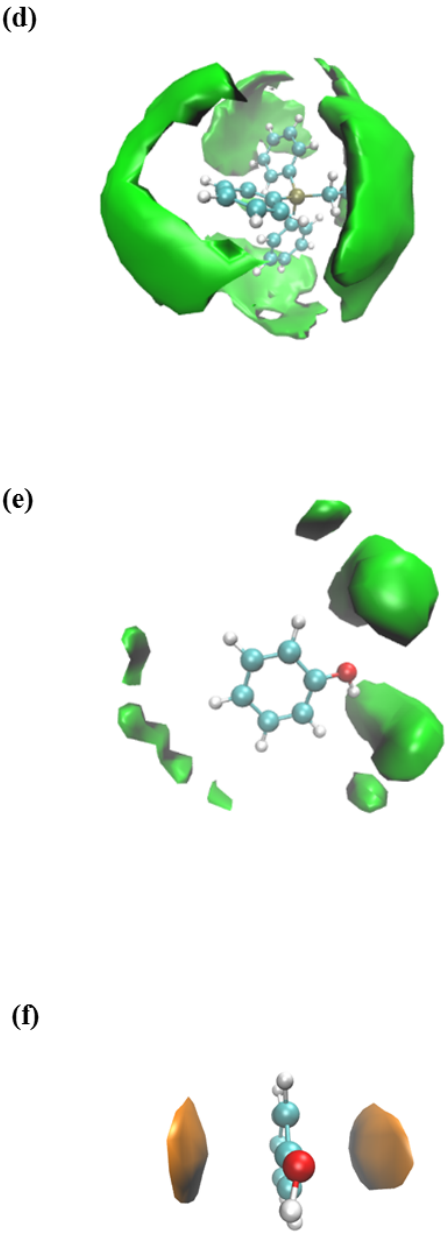
(d)
(e)
(f)

Figure 5

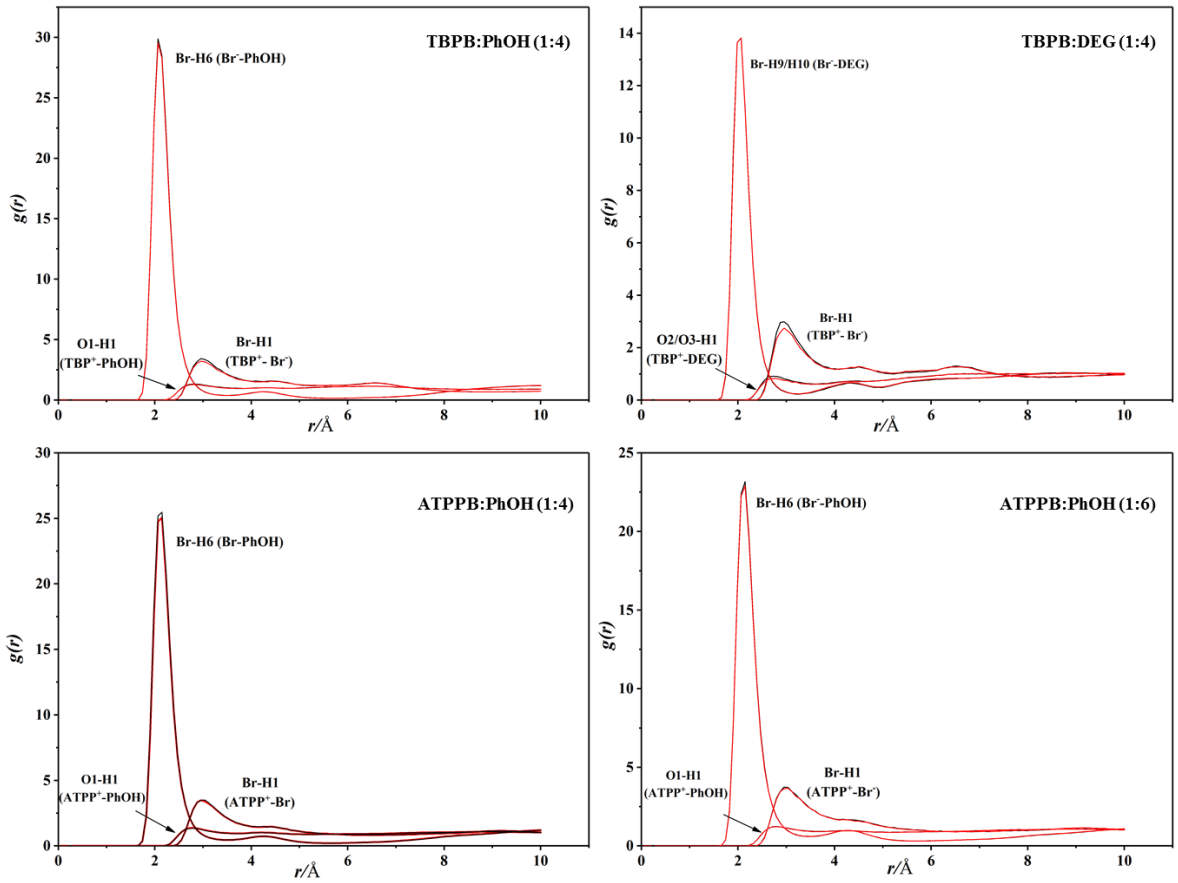
TBPB:PhOH (1:4)
Br-H6 (Br⁻-PhOH)
O1-H1 (TBP⁺-PhOH)
Br-H1 (TBP⁺- Br⁻)
TBPB:DEG (1:4)
Br-H9/H10 (Br⁻-DEG)
O2/O3-H1 (TBP⁺-DEG)
Br-H1 (TBP⁺- Br⁻)
ATPPB:PhOH (1:4)
Br-H6 (Br-PhOH)
O1-H1 (ATPP⁺-PhOH)
Br-H1 (ATPP⁺-Br)
ATPPB:PhOH (1:6)
Br-H6 (Br⁻-PhOH)
O1-H1 (ATPP⁺-PhOH)
Br-H1 (ATPP⁺-Br⁻)
g(r)
r/Å

Figure 6

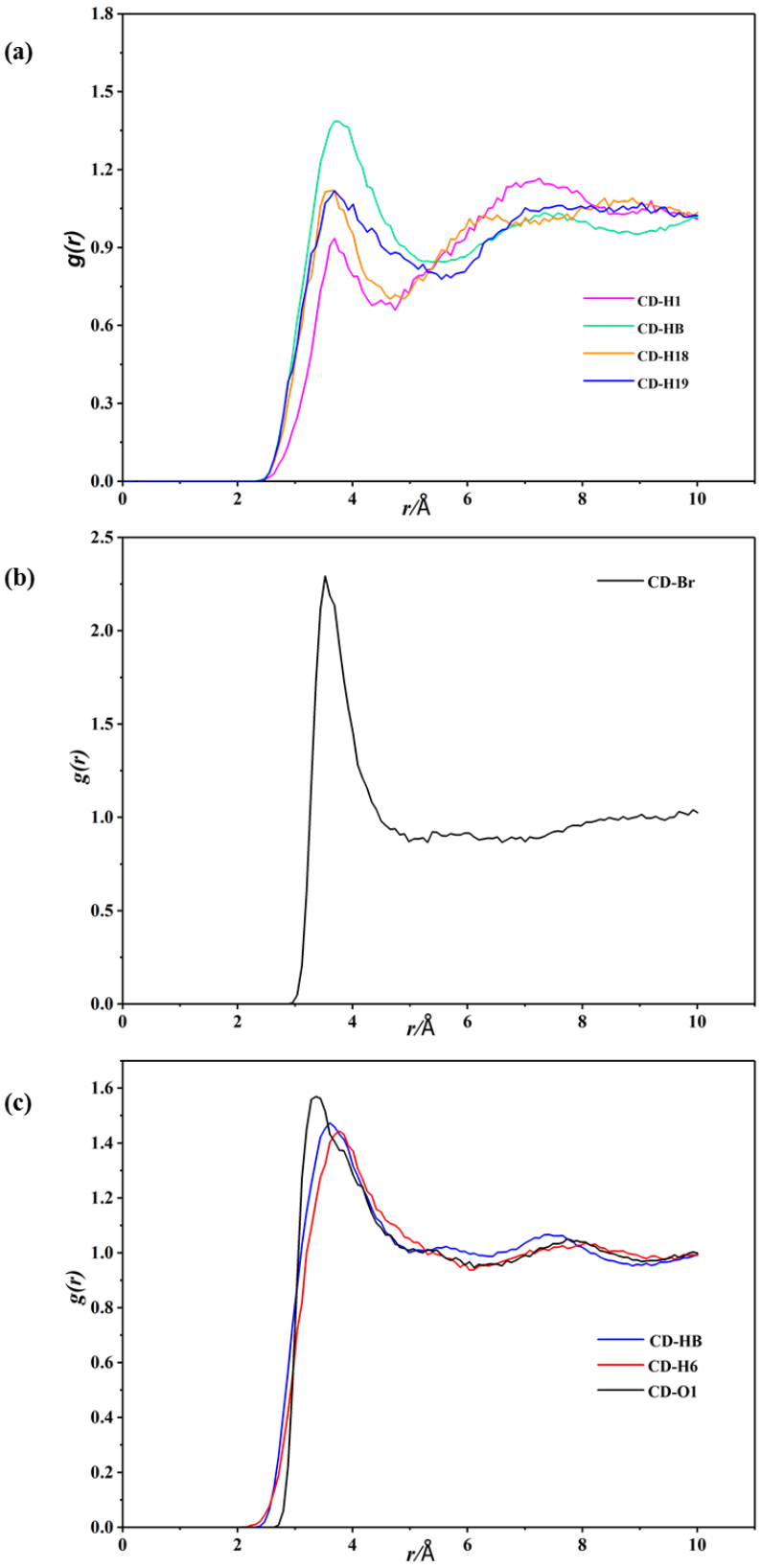

Figure 7

(a)

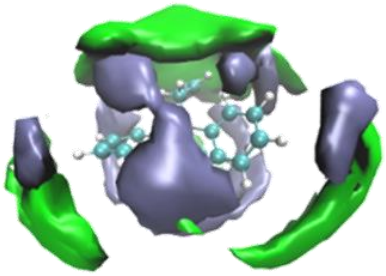

(b)

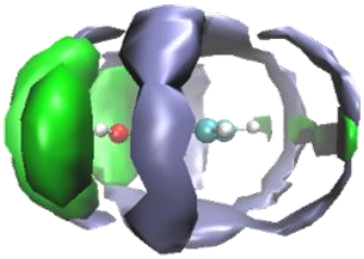

Figure 8

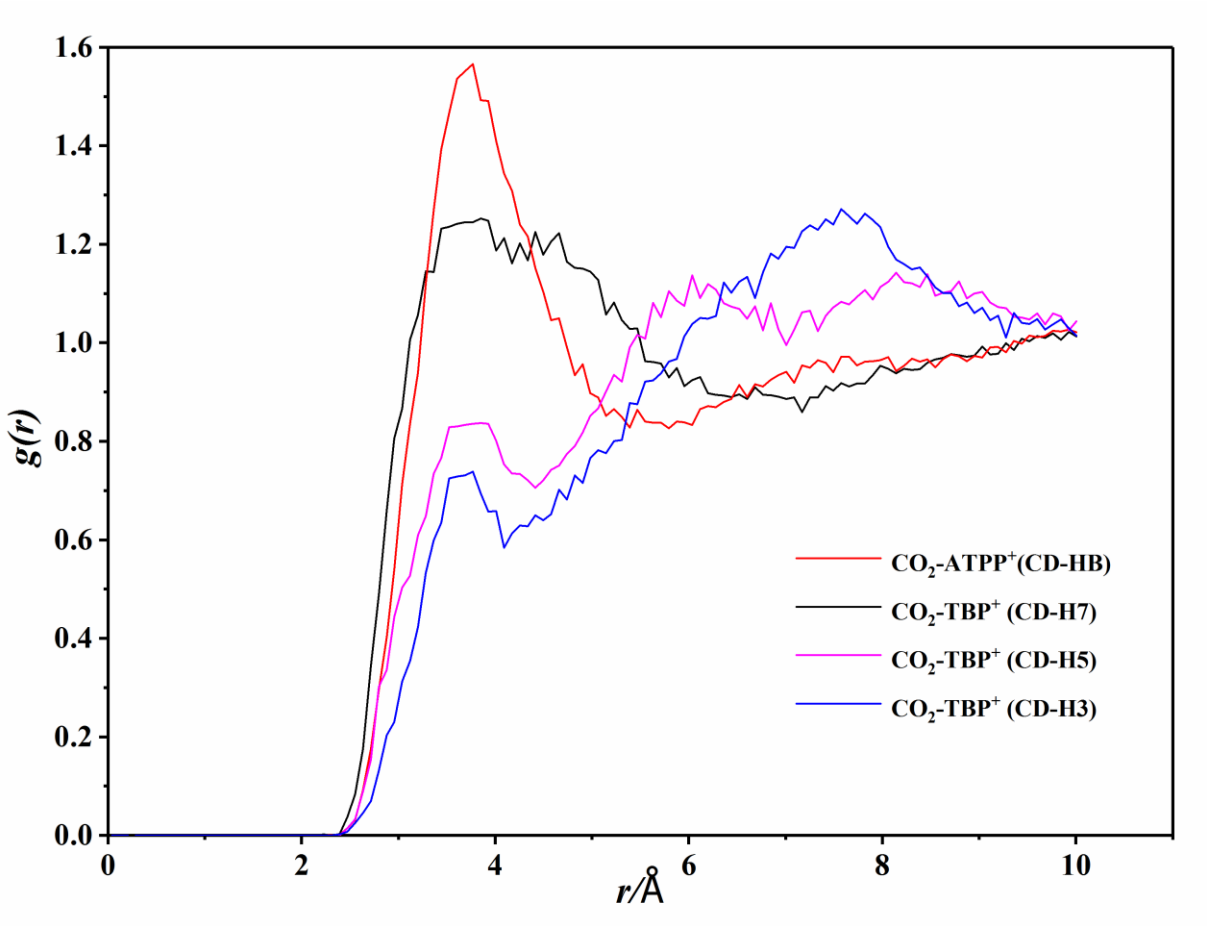
1.6
1.4
1.2
1.0
0.8
0.6
0.4
0.2
0.0
g(r)
0
2
4
6
8
10
r/Å
CO2-ATPP+(CD-HB)
CO2-TBP+ (CD-H7)
CO2-TBP+ (CD-H5)
CO2-TBP+ (CD-H3)

Figure 9

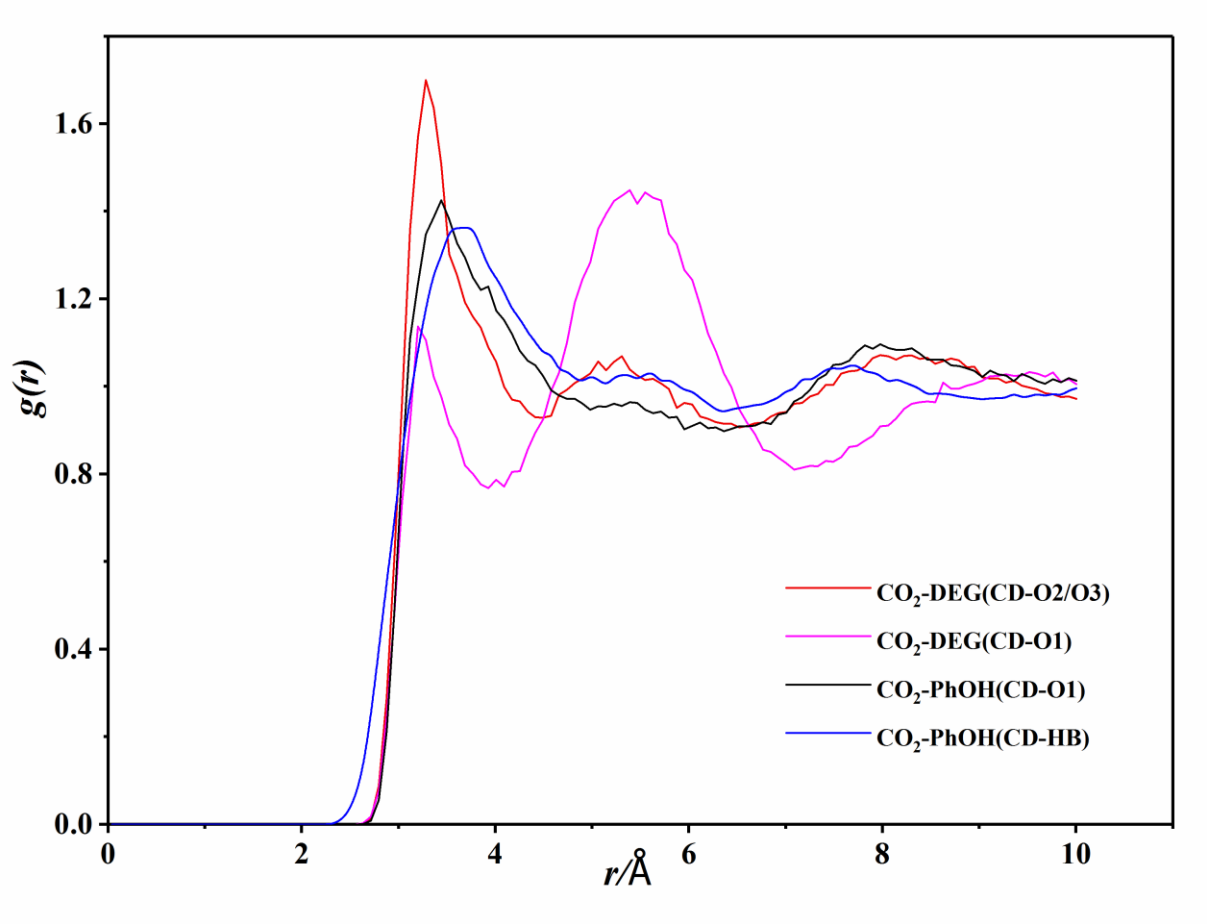
1.6
1.2
0.8
0.4
0.0
g(r)
0
2
4
6
8
10
r/Å
CO2-DEG(CD-O2/O3)
CO2-DEG(CD-O1)
CO2-PhOH(CD-O1)
CO2-PhOH(CD-HB)

Figure 10

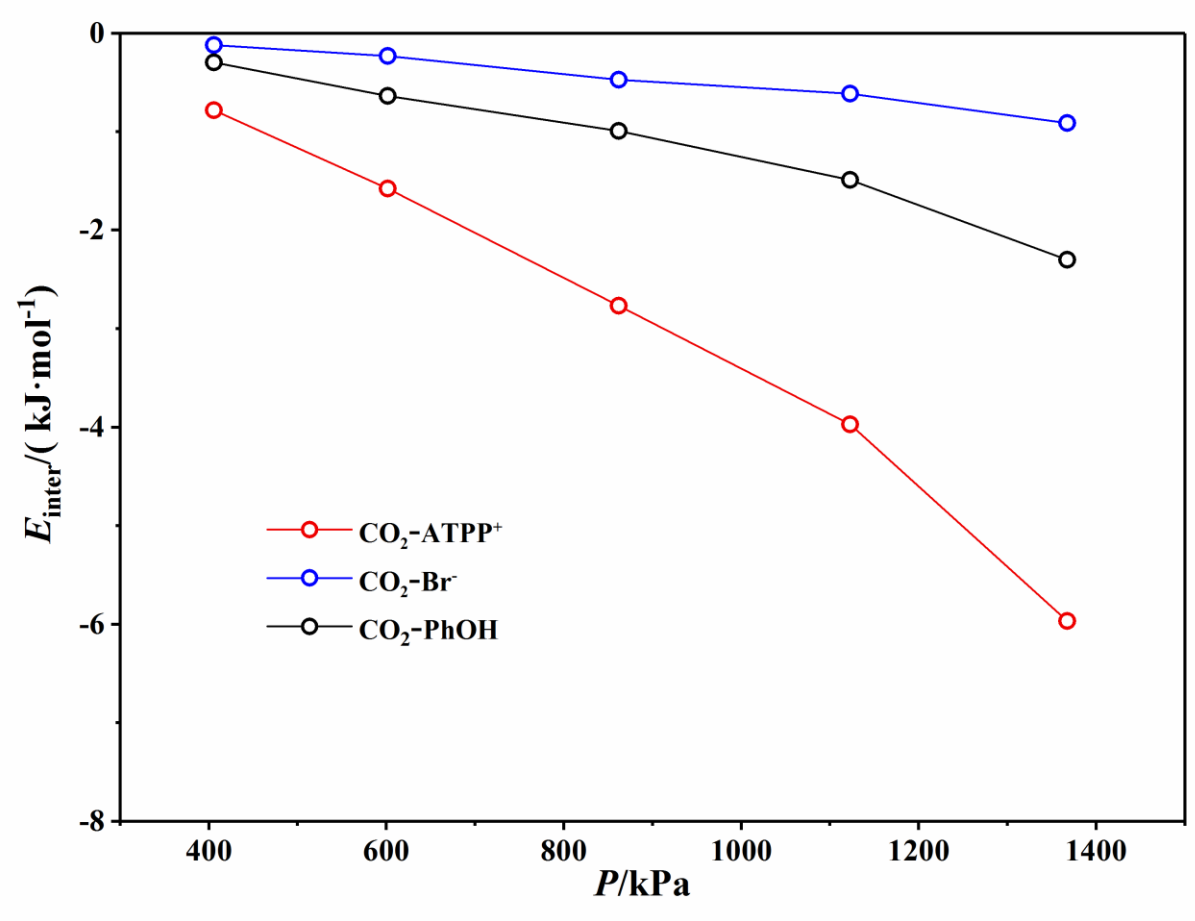
0
-2
-4
-6
-8
400
600
800
1000
1200
1400
P/kPa
E_inter/(kJ·mol-1)
CO2-ATPP+
CO2-Br-
CO2-PhOH

Table of Contents